PHYSICAL REVIEW B **83**, 224504 (2011)

Geometry-driven vortex states in type-I superconducting Pb nanowires

Miles A. Engbarth,[1] Simon J. Bending,[1] and Milorad V. Milošević[2]
[1]*Department of Physics, University of Bath, Claverton Down, Bath BA2 7AY, United Kingdom*
[2]*Departement Fysica, Universiteit Antwerpen, Groenenborgerlaan 171, B-2020 Antwerpen, Belgium*
(Received 9 March 2011; revised manuscript received 27 April 2011; published 21 June 2011)

Hall probe magnetometry has been used to investigate the magnetization of individual cylindrically shaped Pb nanowires grown by electrocrystallization on a highly oriented pyrolytic graphite electrode. These measurements have been interpreted by comparison with three-dimensional Ginzburg-Landau (GL) calculations for nanowires with our sample parameters. We find that the measured superheating field and the critical field for surface superconductivity are strongly influenced by the temperature-dependent coherence length, $\xi(T)$ and penetration depth $\lambda(T)$ and their relationship to the nanowire diameter. As the temperature is increased toward T_c this drives a change in the superconductor-normal transition from first order irreversible to first order reversible and finally second order reversible. We find that the geometrical flux confinement in our type-I nanowires leads to the formation of a one-dimensional row of single-quantum vortices. While GL calculations show a quite uniform distribution of vortices in thin nanowires, clear vortex bunching is found as the diameter increases, suggesting a transition to a more classical type-I behavior. Subtle changes in minor magnetization loops also indicate that slightly different flux configurations can form with the same vorticity, which depend on the sample history.

DOI: 10.1103/PhysRevB.83.224504 PACS number(s): 74.78.−w, 74.70.Ad, 74.25.Ha, 74.20.De

I. INTRODUCTION

Superconductivity is a macroscopic quantum phenomenon characterized by dissipationless supercurrents and perfect diamagnetism. Bulk superconductors are divided into either type I or type II on the basis of their magnetic properties; ideal type-I materials ($\kappa = \lambda/\xi < 1/\sqrt{2}$) exhibit perfect diamagnetism up to a critical field H_c, while type-II materials ($\kappa = \lambda/\xi > 1/\sqrt{2}$) allow the penetration of flux-quantized vortices in the mixed state above a lower critical field H_{c1}. This simple division, however, breaks down completely in mesoscopic superconductors (whose sizes are comparable to the superconducting coherence length) due to boundary conditions imposed on the order parameter by the geometrical confinement as well as surface barriers and demagnetizing effects. We have studied mesoscopic superconductivity in truly three-dimensional disorder-free lead nanowires, grown by electrocrystallization on highly ordered pyrolytic graphite (HOPG) substrates with controllable shapes and sizes. While lead is well known to be a type-I superconductor in bulk form, our Hall micromagnetometry experiments and Ginzburg-Landau simulations clearly demonstrate that geometrical confinement in nanowires leads to intermediate and trapped flux states composed of discrete single-quantum vortices. Underlying such distinctly type-II behavior we nevertheless find characteristic type-I signatures; pairs of vortices are sometimes found to "bind" into vortex molecules, strongly reminiscent of type-1.5 superconductivity that was recently proposed for the two-band superconductor MgB_2,[1] and the hierarchy of observed flux distributions exhibits preferred even-vorticity states.

It is well known that arbitrarily shaped bulk type-I samples do not exhibit perfect diamagnetism all the way up to the critical field H_c. Shape-dependent demagnetizing effects lead to an enhancement of the surface fields and, once these reach H_c, flux penetrates into the body of the sample. The intermediate state formed consists of coexisting superconducting and normal domains, and the latter can have complex structures and topologies, organizing themselves so that the maximum local fields are limited to H_c. Indeed, magneto-optic imaging has recently been used to reconsider the problem of the equilibrium structure of the intermediate state in bulk Pb with compelling new evidence that it corresponds to an array of flux tubes[2] rather than the lamella-like domains proposed by Landau many years ago.[3] Recent modeling of small, although not strictly mesoscopic, type-I superconducting squares[4] reveals complex geometric flux patterns that conform with the square sample symmetry due to interactions with surface barriers. As the size of type-I samples is reduced to mesoscopic dimensions such geometric confinement becomes stronger still. Indeed the intermediate state may even become energetically unstable, while superconductivity can actually be enhanced at surfaces which are parallel to an applied magnetic field (surface superconductivity). As a consequence the flux structures formed become intimately dependent on the size, shape, and symmetry of the samples investigated. This is particularly pronounced in our nanowire samples with the magnetic field perpendicular to the axis, a situation with a pronounced one-dimensional character and twofold symmetry.

Many important investigations of mesoscopic superconductors have been reported to date, but nearly all have used nanopatterned polycrystalline films[5–7] in which disorder and thin film geometry lead to type-II behavior. Recent breakthroughs in electrocrystallization on HOPG substrates,[8] however, allow one to grow single-crystal lead nanowires that are clean enough and wide enough to remain type I, but small enough to exhibit striking mesoscopic effects. We have used Hall array nanomagnetometry to measure the magnetic response of individual Pb nanowires. Many prior theoretical investigations have focused on calculations of the properties of mesoscopic superconductors based on solutions of the nonlinear Ginzburg-Landau (GL) equations for two-dimensional (2D) sample geometries;[9–12] only more recently has this method been extended to truly 3D cases.[13] Here our experiments have been simulated using fully

three-dimensional Ginzburg-Landau calculations, yielding powerful insights into the flux structures formed as well as the magnetic field and order parameter distributions.

II. METHODS

The Pb nanowires studied here were grown by electrodeposition onto a highly oriented pyrolytic graphite electrode [Fig. 1(a)]. An electrolyte of 5 mM lead nitrate was used with a supporting electrolyte of 0.1M boric acid. Solutions were freshly made from high-purity 99.999% reagents with Milli-Q water (resistivity >18.2 MΩ cm^{-1}). The wires were grown by applying a reduction potential of -1.5 V versus an Ag/AgCl reference electrode for 60 s using a computer-controlled potentiostat. Nanowires fabricated this way are typically $\sim$10–20 μm long and have diameters in the range 100–500 nm [Figs. 1(c) and 1(d)].

Magnetometry measurements were carried out using a linear array of 1×1 μm^2 GaAs/AlGaAs heterostructure Hall probes [Fig. 1(b)]. Nanowires are placed onto the Hall probes under a long-focal-length optical microscope using a nylon hair that has a tip approximately 500 nm wide attached to a piezoelectric nanomanipulator with a 200 nm minimum step size. The nanowires readily stick to the nylon hair when being removed from the HOPG, but getting them off the hair onto the Hall probes is more challenging. We achieve this by melting a small amount of paraffin wax on the Hall probes, which helps to pull the nanowires off the hair when they come into contact and also acts as a lubrication medium allowing the nanowire to be pushed around on the surface and into position over the Hall cross. The majority of the wax evaporates before it resolidifies; the small amount left sticks the nanowire in place. The Hall sensors were operated with a 20 μA 32 Hz ac current and the Hall voltage detected with a lock-in amplifier. An external magnetic field was applied perpendicular to the Hall array using a superconducting magnet that was situated along with the sample in a liquid-helium bath cryostat.

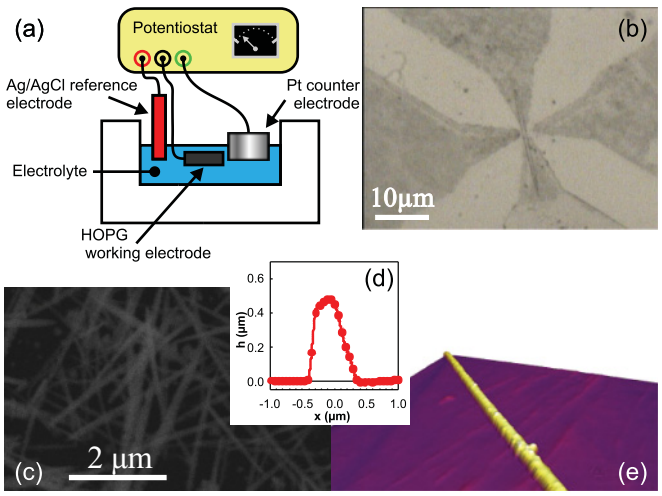

FIG. 1. (Color online) (a) Schematic diagram of electrochemical setup. (b) Optical micrograph of Hall probe with a Pb nanowire in position. (c) Scanning electron micrograph of a typical array of Pb nanowires deposited on a HOPG electrode. (d) Atomic force microscope (AFM) topographic profile across a typical Pb nanowire. (e) 3D AFM rendering of a typical Pb nanowire.

The 3D GL calculations were performed in the London gauge, div$\vec{A} = 0$, using dimensionless variables such that distances are measured in units of ξ and the superconducting order parameter is scaled to its value in the absence of the magnetic field. The Neumann boundary condition at the sample surface takes the form $(-i\vec{\nabla}_{3D} - \vec{A})\Psi|_{\text{boundary}} = 0$ and the GL equations are solved self-consistently in Cartesian coordinates on a uniform cubic grid with a typical grid spacing of less than 0.2λ (In type-I superconductors, λ is the shortest lengthscale, and sufficient number of grid points per λ is essential for the precision of the numerical calculation). More details of the numerical method are given in Refs. 13 and 14. In addition, we consider also the fluctuations of the order parameter, introduced as white noise in the GL formalism, in the same manner as done previously in Ref. 15.

III. RESULTS

Figure 2(a) shows several magnetization loops for a 390-nm-diameter nanowire at different temperatures where the bulk critical fields $H_c(T)$ are indicated by vertical dashed lines. In a bulk sample with the same shaped cross section we would expect to see fully reversible magnetization due to the absence of the geometrical barrier in this cylindrical geometry.[16–18] Here, however, we see a large degree of irreversibility, resulting from important superheating and surface superconductivity effects in mesoscopic samples. The ability to superheat a superconducting sample requires any surface defects to be smaller than the superconducting coherence length[19] and hence the phenomenon is not usually observed in bulk samples where it is very difficult to achieve such high-quality surfaces. Surface superconductivity ultimately plays a much stronger role here than in bulk samples because the surface-to-volume ratio is so much larger in mesoscopic samples. As the applied field is increased from zero in all cases the superconducting state is seen to survive to well above $H_c(T)$, clearly highlighting the role that superheating and surface superconductivity (that leads to a small tail in the diamagnetic response at the end of the main superconductor-normal transition for $T \leqslant 5.6$ K) play in our nanowires.

Surface superconductivity is theoretically expected to survive up to $H_{c3} \sim 2.39\kappa H_c$,[22] for a planar interface, where κ is the Ginzburg-Landau parameter and is known to have quite a strong temperature dependence in Pb; $\kappa \sim 0.45$ at $T \sim 3$ K and $\kappa \sim 0.3$ at $T \sim T_c$. The exact temperature dependence of κ is not well known, especially for mesoscopic samples, but Stenuit *et al.*[23] found that in their Pb nanowires $\lambda(T)$ is best approximated by the Gorter-Casimir two-fluid model where

$$\lambda(t) = \frac{\lambda(0)}{\sqrt{1-t^4}}, \tag{1}$$

where $t = T/T_c$. This, combined with the Ginzburg-Landau temperature dependence of $\xi(T)$,

$$\xi(t) = \frac{\xi(0)}{\sqrt{1-t}}, \tag{2}$$

implies that $\kappa(t)$ will fall with temperature as $\kappa(0)[(1+t)(1+t^2)]^{-1/2}$. This dependence of κ on temperature in

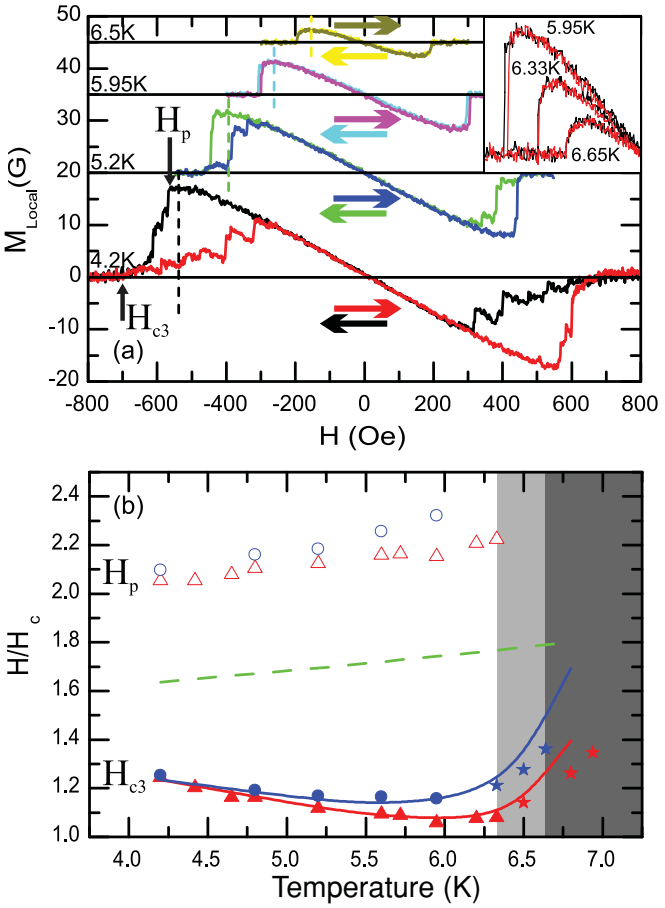

FIG. 2. (Color online) (a) Magnetization curves at various temperatures for a 390-nm-diameter nanowire. Dashed vertical lines show the bulk values of H_c. Labeled arrows illustrate the points taken for H_{c3} and H_p as described in the text. Inset shows *M*-*H* loops at various temperatures illustrating the change in the superconductor-normal transistion from first order irreversible to second order reversible. (b) Temperature-dependent superheating field (H_p, open symbols after correction by a demagnetization factor) and critical field for surface superconductivity (H_{c3}, solid symbols) for nanowires with diameters of 390 nm circles) and 470 nm (triangles). Solid lines show calculations of H_{c3} for a slab with the same thickness due to Fink (Ref. 20) after scaling by a factor of 1.25 (see text). The dashed line shows the calculated $H_p(T)$ due to Matricon and Saint-James (Ref. 21). Stars show values of H_{c3} in the regime where the magnetization curves become reversible.

Pb results in the unusual situation that H_{c3} exceeds H_c at low temperatures but falls below it near T_c when surface superconductivity no longer plays a role and the transition to the normal state becomes abrupt. This is further complicated in the mesoscopic regime by additional enhancements of surface superconductivity when the coherence length becomes comparable to the size of the superconductor.[20,24] For example, in a thin slab in a parallel field this enhancement is predicted to occur once the slab thickness is less than $\sim 2.5\xi(T)$, when H_{c3} starts to increase rapidly with increasing confinement (smaller thickness). Above this critical value H_{c3} is effectively independent of slab thickness. As the temperature increases the coherence length ξ diverges as the temperature approaches the critical temperature T_c. In our measurements we define H_{c3} as the point at which the magnetization deviates from zero for decreasing fields. Our nanowires are thick enough that confinement effects are negligible at very low temperature yet thin enough that these effects become significant at higher temperatures, even when T is not very close to T_c. As the temperature increases, the combination of decreasing κ and enhancement of H_{c3} at higher values of T leads to the situation shown in Fig. 2(b) where we compare H_{c3} (normalized by the bulk H_c) for two nanowires with different diameters d. Here we can see that as T is increased there is an initial decrease in H_{c3} due to the decrease of κ, before this trend is reversed due to the rapid increase in ξ close to T_c. As expected, the enhancement of H_{c3} is more pronounced for the thinner nanowire, but both nanowires have roughly the same value of H_{c3} at 4.2 K where d/ξ is too large to influence this.

The temperature dependence of κ also influences the superheating field, which is known to increase approximately as $\kappa^{-0.5}$ for $\kappa \ll 1$.[21] In order to determine if the superconductor exhibits superheating we must compare the field at which quantized flux first penetrates, H_p, to the value expected when the sample's demagnetization factor is taken into account. The demagnetization factor for a bulk cylinder in a perpendicular magnetic field is 0.5, indicating that the magnetic fields at the surface are enhanced by a factor of 2. This leads us to expect the first penetration of flux and formation of an intermediate state in our nanowires at $H = 0.5H_c$. In practice we only observe intermediate states for increasing fields at $T \leqslant 5.6$ K and always at $H_p > H_c$ just before the nanowire is driven completely normal. H_p is shown in Fig. 2(b) for two different nanowires (again normalized by the bulk H_c and corrected by the estimated demagnetization factor). H_p is the point where the magnetization deviates abruptly from the Meissner background.

Figure 2(b) also includes predicted behaviors for both H_{c3} (solid lines) and H_p (dotted line). The expected dependence of H_{c3} on T was deduced from Fink's calculation of H_{c3} versus d/ξ for a thin slab,[20] while that of H_p was determined from the dependence of the superheating field on κ given by Matricon and Saint James.[21] We have assumed the $\kappa(T)$ dependence given above, setting $\kappa(T_c)$ to 0.3, a value that is reasonable for a disorder-free single-crystalline Pb nanowire. While the theoretical estimates of H_{c3} and H_p are in good qualitative agreement with experimental data, both underestimate the measured values by a factor of approximately 1.25 at 4.2 K. The discrepancy in H_{c3} is likely to be due to additional enhancements in our cylindrical nanowires as compared to the slab geometry of the model used. Given that our Pb samples are not truly in the limit $\kappa \ll 1$, discrepancies in the calculated superheating fields are also not surprising. We note that H_p is larger in the thinner nanowire, and in both nanowires the rate at which H_p increases with T near T_c is far greater than predicted. Numerical calculations by Landau and Rinderer[25] for superconducting slabs with somewhat smaller values of κ actually show a pronounced reduction of the superheating field for thickness $d < 20\lambda_L(T)$, passing through a minimum near $d_c \sim 4\lambda_L(T)$ and then rising again for still smaller thicknesses. Since this predicts the opposite trend to that observed, it suggests the presence of additional size-dependent mesoscopic effects that *suppress* the penetration of flux in our nanowire samples.

Flux entering a superheated type-I superconductor would be expected to drive it normal; however, surface superconductivity prevents this from happening, allowing a few flux quanta to enter without turning the whole sample normal. Furthermore, it is known that flux within a superconductor can reinforce surface barriers in mesoscopic samples,[26] allowing for further superheating of the intermediate state before it eventually becomes unstable, leaving only surface superconductivity, which will be strongest near the sharp corners at the ends of the nanowire. The complete disappearance of the intermediate state, at $T > \sim 6.1$ K for the thin nanowire and $T > \sim 6.4$ K for the thicker nanowire, can be attributed to divergence of the coherence length as the critical temperature is approached, eventually leading to a situation where $\xi(T)$ becomes comparable to or larger than the width of the nanowire. At this point the nanowire is narrower than the superconductor/normal interface, normal regions inside the sample can no longer be supported, and the intermediate state becomes unstable. As the temperature increases further λ will also become comparable to the width of the nanowires. The associated increase in penetration of magnetic field makes itself apparent by the increased rounding of the magnetization curves near the critical field. Indeed, it is predicted that when the width of a type-I slab drops below $\sqrt{5}\lambda(T)$ the phase transition from the superconducting to the normal state becomes second order[27] and the discontinuous jump in magnetization at H_c disappears. These various stages can be seen clearly in the inset for Fig. 2(a), where the transition is initially first order and irreversible at $T < 5.95$ K, becoming fully reversible as the temperature increases and the intermediate state is lost, before finally becoming second order at $T > 6.65$ K. This is highlighted in Fig. 2(b) by the shaded areas which serve as a rough guide to the temperatures at which these changes in behavior can be observed, although the exact point is clearly dependent on the nanowire thickness. A similar effect has been seen by Geim *et al.*[6] as the size of Al superconducting disks was reduced at a fixed temperature.

As the magnetic field is reduced for a nanowire in the normal state, surface superconductivity will first nucleate around the ends and then spread along the edges before joining up in the middle. Flux through the nanowire is not fully quantized until this happens, a situation that can be recognized by the appearance of definite steps in the magnetization curve. Reducing the field from the normal state, we observe metastable trapped flux states for $T \leqslant 6.1$ K that exist down to fields well below the bulk $H_c(T)$. In this temperature range the system is seen to switch between hierarchies of flux states with progressively reduced vorticity until eventually jumping back to the Meissner state. Transitions between these trapped flux configurations require the system to overcome barriers between them, and increased thermal fluctuations at higher temperatures greatly reduce their ranges of metastability.

In order to better understand how our magnetization curves relate to the flux distribution within our samples, we have performed a series of 3D GL calculations on cylinders with similar diameters to our nanowires. Computational overheads restrict us to simulations of cylinders that are 1.8 μm long; the calculations for stray magnetic fields are then averaged over the area of the Hall probe to approximate the exact experimental

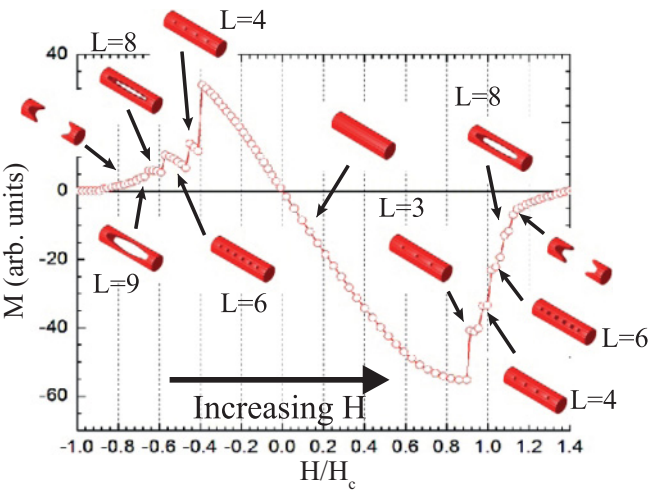

FIG. 3. (Color online) 3D GL simulations for a 500-nm-diameter cylinder of length 1.8 μm at 4.2 K with $\kappa = 0.3$. Shown are the calculated magnetization curve and 3D Cooper-pair density plots at the indicated values of magnetic field.

conditions. The first simulation is shown in Fig. 3 for a 500-nm-diameter cylinder at 4.2 K with $\xi = 118$ nm and $\kappa = 0.3$, this is slightly wider than any of the nanowires we have measured and so the results cannot be directly compared, but is useful in allowing us to visualize the possible flux evolution inside a nanowire and replicates many of the features seen in our magnetization curves. We have included 3D Cooper-pair density plots for each vorticity state L, and from these we can relate the progression of the flux distribution to specific features in the magnetization curves. For instance, we can clearly see the nucleation of superconductivity at the ends that spreads along the edges before encircling the whole sample. At this point the enclosed flux becomes quantized and changes in magnetization proceed in a more steplike fashion, mirroring what is observed in experimental data. As the applied field approaches H_c from the Meissner state, we see a large amount of superheating and flux penetrating above H_c without driving the whole sample normal, i.e., a superheated intermediate state, again similar to our experimental data. We also note that most of the stable vorticity states are even, and frequently undergo transitions involving the penetration or expulsion of *two* flux quanta.

Figures 4(a)–4(d) show minor magnetization loops traced near the superconductor-normal transition from different starting points. Loops start either in the Meissner state or in the normal state and are tracked to specific metastable states and then the sweep direction is reversed in order to determine the stability range of each state. Since the Hall sensor only captures flux from a small fraction of the nanowire, it is difficult to assign exact flux distributions to experimentally observed states. Broadly speaking, minor loops that start in the Meissner state approximately overlay those that start from the normal state, but there are several subtle differences which indicate that the flux configurations are not exactly the same in both cases. For example, the trace that starts in the Meissner state and backtracks from the intermediate state at 5.2 K in Fig. 4(a) appears to overlap the trace from the normal state, but does not jump back to the Meissner state until a

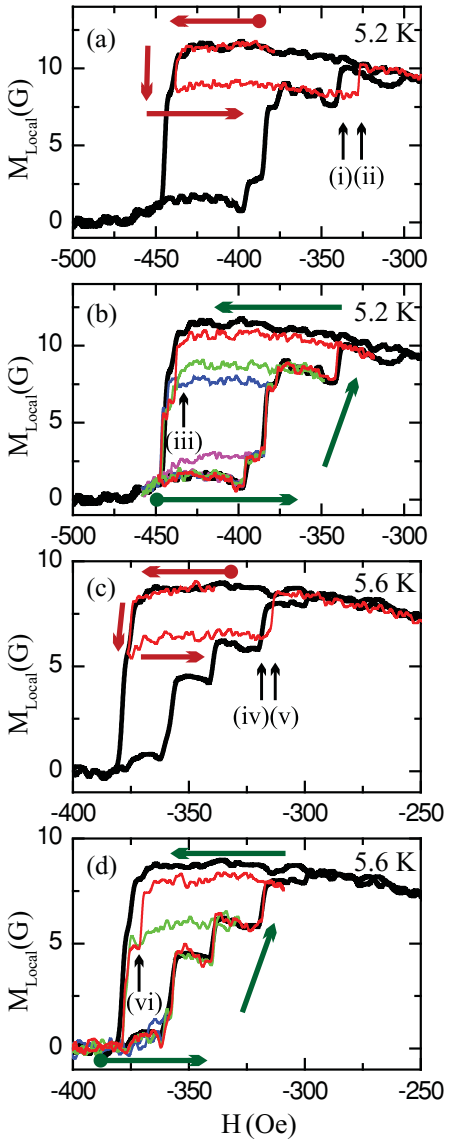

FIG. 4. (Color online) Minor magnetization loops for the 390-nm-diameter nanowire tracing out the stability range of each vorticity state (as indicated by different light weight lines) superimposed on the full magnetization curve (heavy weight line). The heavy bold arrows indicate the direction of field sweep with the circles showing the start point. The lighter-weight arrows labelled (i)–(vi) relate to points explained in the text.

somewhat lower field as highlighted at points (i) and (ii). Also the minor loop from the normal state in Fig. 4(b) that reaches the same apparent plateau as the minor loop from the Meissner state in Fig. 4(a) does not backtrack all the way to the main superconducting-normal transition, but switches at point (iii) to a higher-vorticity intermediate state. Both observations suggest that the two different minor loops prepare slightly different flux configurations, and these differences are located quite far from the Hall sensor. At the higher temperature of 5.6 K shown in Fig. 4(c), states starting from the Meissner state and the normal state clearly no longer coincide, and again are stable up to different applied fields indicated by points (iv) and (v). In this case, however, all branches appear to forward- and backtrack to the same apparent set of

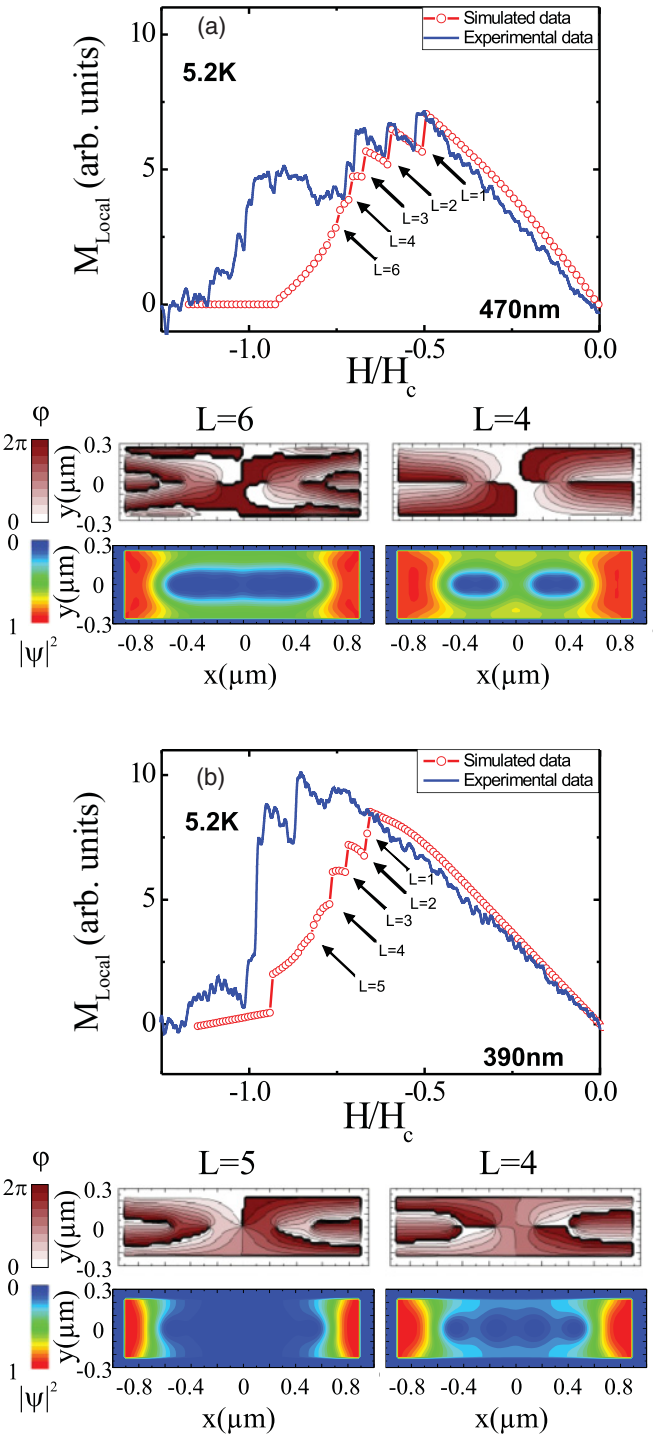

FIG. 5. (Color online) Comparison of the measured nanowire M-H loops with GL simulations of magnetisations for cylinders with the same diameter for (a) a 470 nm nanowire and (b) a 390 nm nanowire. Also shown are the calculated Cooper pair density plots, $|\psi|^2$, and phase plots, φ, for selected values of L.

intermediate states as shown in Fig. 4(d). However, backtracked plateaus are not all stable out to the main superconducting-normal transition. Indeed, the central trapped flux state suddenly increases its vorticity upon backtracking to higher fields and appears to fall onto the lower trapped flux branch in Fig. 4(d) at point (vi).

It is not possible to determine the exact distribution of flux within the nanowires from our magnetization measurements alone. The nanowires investigated here are $\sim$20 μm long while we are only able to directly observe the magnetization of the central $\sim$1–2 μm. In order to overcome this limitation we have performed a second set of 3D GL calculations for cylinders with the same diameters as our nanowires, allowing us to make a more direct comparison between the two sets of results. This is illustrated in Fig. 5, where we compare measured and calculated data for 390- and 470-nm-diameter Pb nanowires at 5.2 K with $\xi = 148$ nm and $\kappa = 0.28$. Again we are restricted to simulations of cylinders that are 1.8 μm long. While there is a large difference in length of the two systems, we can expect good agreement for low values of L since flux will first penetrate near the middle of the nanowire where confinement due to the ends is weak. For higher values of L there is a greater compression of flux in the simulated wire than in the measured nanowire, making it more difficult to compare the two directly. For instance, in Fig. 5(a) it can be seen that the $L = 4$ state appears to be much more stable experimentally than in the simulated data. It is, however, almost certain that the longer length of the measured nanowire allows vortex populations to change far from the Hall sensor that do not appear to influence the recorded magnetization data, or the apparent vorticity.

Agreement between simulation and experiment is not as good for the thinner 390-nm-diameter nanowire shown in Fig. 5(b). However, in both cases we see an abrupt discontinuous jump to the superconducting state as the field is increased toward zero, in stark contrast to the rather gradual onset that was observed in the thicker nanowire. Also, the intermediate state is stable over a much narrower field range in both the experimental and simulated data when compared to the thicker nanowire due to the much stronger lateral confinement, making flux expulsion easier in this case.

As well as allowing us to estimate different values of vorticity L from our measured magnetization data, GL simulations are especially useful in determining the likely distribution of flux within the nanowires. Cooper-pair density plots, as shown in Fig. 5, highlight the effect of the extreme quantum confinement in our nanowire geometry. Unlike the intermediate state in bulk type-I superconductors, which form large normal domains containing multiple flux quanta, here normal regions are "squeezed" such that only single flux vortices can form in chains along the long axis of the nanowire. This is not always clear for large L from the Cooper-pair plots, but can be confirmed by referring to the adjacent corresponding phase plots of the superconducting order parameter.

If we could gradually increase the diameter of the nanowire from the values investigated here we would expect to see a crossover at which the behavior reverts to that of a classic type-I superconductor with multiquanta intermediate domains. We do indeed see evidence for this broad trend in our measurements. The flux distribution in the thin nanowire is seen to approximate that of a type-II superconductor with evenly spaced single-quantum vortices. For the thicker nanowire, however, we observe something intermediate between type-I and type-II behaviors. Although we still observe a chain of single-quantum vortices, these are not uniformly distributed along the length of the nanowire; rather they form bunches (in this case pairs) that are reminiscent of the normal domains in macroscopic type-I superconductors as well as the recently proposed type-1.5 superconductivity. Such bunching is also found to promote even-vorticity states and explains the absence of some odd-vorticity states (e.g., $L = 5$) in the thicker nanowire.

IV. CONCLUSIONS

We have exploited recent developments in electrocrystallization to fabricate superconducting Pb nanowires with diameters of around 400 nm and lengths of approximately 20 μm. Hall probe magnetometry has been used to directly measure the "local" magnetization of the central region of these nanowires, allowing us to determine the superheating field as well as the critical field for surface superconductivity. We demonstrate explicitly how these parameters are influenced by the temperature dependencies of the penetration and coherence lengths and their relationship to the diameter of the nanowire. At high temperatures, as these length scales approach the nanowire diameter, we observe a change in the superconductor-normal transition from first order irreversible to first order reversible and finally second order reversible. This occurs at the same time that κ is falling with increasing temperature, making the nanowire more type I.

By comparing our measured results with GL calculations we have been able to show that geometrical flux confinement within our type-I nanowires leads to the formation of a 1D row of single-quantum vortices. While the GL calculations show a quite uniform distribution of vortices in the thinner nanowire, clear bunching of vortices is found in the thicker nanowire, suggesting a transition to more classical type-I behavior as the diameter increases. Bunching is found to promote even-vorticity states and explains the absence of some odd-vorticity states in the thicker nanowire. By measuring minor magnetization loops we were able to investigate the stability range of different vorticity states. Subtle changes in these minor loops for different start and end points of the field sweep suggest that slightly different flux configurations can form with the same vorticity, which depend on the sample history.

ACKNOWLEDGMENTS

We acknowledge valuable conversations with F. V. Kusmartsev and W. M. Wu at Loughborough University, UK This work was supported by the EPSRC-UK under Grant No. EP/E039944/1, and the Flemish Science Foundation (FWO).

[1] V. Moshchalkov, M. Menghini, T. Nishio, Q. H. Chen, A. V. Silhanek, V. H. Dao, L. F. Chibotaru, N. D. Zhigadlo, and J. Karpinski, Phys. Rev. Lett. **102**, 117001 (2009).

[2] R. Prozorov, A. F. Fidler, J. R. Hoberg, and P. C. Canfield, Nature Physics **4**, 327 (2008).

[3] L. D. Landau, Phys. Z. Sowjet. **11**, 129 (1937).

[4] A. D. Hernández and D. Domínguez, Phys. Rev. B **72**, 20505 (2005).
[5] V. Moshchalkov, L. Gielen, C. Strunk, R. Jonckheere, X. Qiu, C. Van Haesendonck, and Y. Bruynseraede, Nature **373**, 319 (1995).
[6] A. K. Geim, I. V. Grigorieva, S. V. Dubonos, J. G. S. Lok, J. C. Maan, A. E. Filippov, and F. M. Peeters, Nature **390**, 259 (1997).
[7] A. Kanda, B. J. Baelus, F. M. Peeters, K. Kadowaki, and Y. Ootuka, Phys. Rev. Lett. **93**, 257002 (2004).
[8] Z. L. Xiao, C. Y. Han, W. K. Kwok, H. H. Wang, U. Welp, J. Wang, and G. W. Crabtree, J. Am. Chem. Soc. **126**, 2316 (2004).
[9] V. A. Schweigert and F. M. Peeters, Phys. Rev. B **57**, 13817 (1998).
[10] V. A. Schweigert, F. M. Peeters, and P. S. Deo, Phys. Rev. Lett. **81**, 2783 (1998).
[11] J. J. Palacios, Phys. Rev. B **58**, 5948 (1998).
[12] J. J. Palacios, Phys. Rev. Lett. **84**, 1796 (2000).
[13] B. Xu, M. V. Milošević, and F. M. Peeters, Phys. Rev. B **77**, 144509 (2008).
[14] G. R. Berdiyorov, A. D. Hernandez, and F. M. Peeters, Phys. Rev. Lett. **103**, 267002 (2009).
[15] M. V. Milošević and F. M. Peeters, Phys. Rev. Lett. **94**, 227001 (2005).
[16] J. Provost, E. Paumier, and A. Fortini, J. Phys. F **4**, 439 (1974).
[17] J. R. Clem, R. P. Huebener, and D. E. Gallus, J. Low Temp. Phys. **12**, 449 (1973).
[18] R. Prozorov, Phys. Rev. Lett. **98**, 257001 (2007).
[19] J. Feder and D. S. McLachlan, Phys. Rev. **177**, 763 (1969).
[20] H. J. Fink, Phys. Rev. **177**, 732 (1969).
[21] J. Matricon and D. Saint-James, Phys. Lett. A **24**, 241 (1967).
[22] D. Saint-James and P. G. De Gennes, Phys. Lett. **7**, 306 (1963).
[23] G. Stenuit, S. Michotte, J. Govaerts, and L. Piraux, Supercond. Sci. Technol. **18**, 174 (2005).
[24] V. A. Schweigert and F. M. Peeters, Phys. Rev. B **60**, 3084 (1999).
[25] I. L. Landau and L. Rinderer, J. Low Temp. Phys. **100**, 219 (1995).
[26] A. D. Hernández and D. Domínguez, Phys. Rev. B **65**, 144529 (2002).
[27] M. Tinkham, *Introduction to superconductivity* (McGraw-Hill, 1996).